ACS APPLIED MATERIALS & INTERFACES

Research Article

www.acsami.org

Hierarchical Core–Shell Carbon Nanofiber@$ZnIn_2S_4$ Composites for Enhanced Hydrogen Evolution Performance

Yajie Chen,[†] Guohui Tian,*[,†,‡] Zhiyu Ren,[†] Kai Pan,[†] Yunhan Shi,[†] Jiaqi Wang,[†] and Honggang Fu*[,†]

[†]Key Laboratory of Functional Inorganic Material Chemistry, Ministry of Education of the People's Republic of China, Heilongjiang University, Harbin 150080, People's Republic of China

[‡]Key Laboratory of Chemical Engineering Process & Technology for High-efficiency Conversion, College of Heilongjiang Province, School of Chemistry and Materials Science, Heilongjiang University, Harbin 150080, China

Supporting Information

ABSTRACT: Improvement of hydrogen evolution ability is an urgent task for developing advanced catalysts. As one of the promising visible-light photocatalysts, $ZnIn_2S_4$ suffers from the ultrafast recombination of photoinduced charges, which limits its practical application for efficient solar water splitting. Herein, we reported a two-step method to prepare hierarchical core–shell carbon nanofiber@$ZnIn_2S_4$ composites. One-dimensional carbon nanofibers were first prepared by electrospinning and carbonization in N_2. The subsequent solvothermal process led to the in situ growth of $ZnIn_2S_4$ nanosheets on the carbon nanofibers to fabricate hierarchical structure composites. The hierarchical core–shell configuration structure can help to form an intimate contact between the $ZnIn_2S_4$ nanosheet shell and the carbon nanofiber backbone compared with the equivalent physical mixture and can facilitate the interfacial charge transfer driven by the excitation of $ZnIn_2S_4$ under visible-light irradiation. Meanwhile, the ultrathin $ZnIn_2S_4$ nanosheets were uniformly grown on the surface of the carbon nanofibers, which can avoid agglomeration of $ZnIn_2S_4$. These synergistic effects made this unique hierarchical structure composite exhibit a significantly higher visible-light photocatalytic activity toward hydrogen evolution reaction compared with pure $ZnIn_2S_4$ or a physical mixture of $ZnIn_2S_4$ and carbon nanofibers in the absence of noble metal cocatalysts.

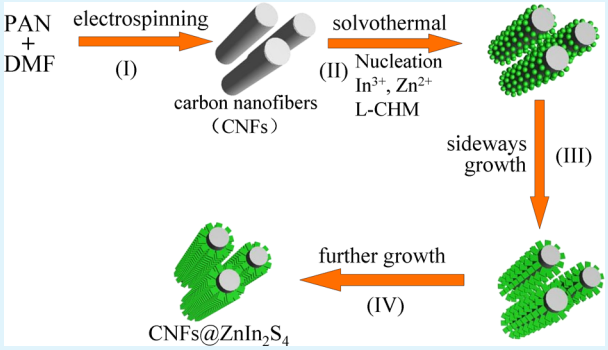

KEYWORDS: *hierarchical structure, core–shell, $ZnIn_2S_4$, carbon nanofiber, composites, photocatalytic hydrogen evolution*

1. INTRODUCTION

In recent years, photocatalytic H_2 production from water splitting has attracted great attention because it is a clean, economical, and environmentally friendly strategy to convert sustainable solar energy into preservable H_2.[1−3] Compared with the conventional wide-band-gap semiconductors, which can solely absorb the UV light and greatly restrict its practical applications, metal sulfides have been intensively studied in photocatalysis because of their suitable band gap and catalytic functions.[4−7] In particular, ternary metal sulfide $ZnIn_2S_4$, which is an eco-friendly and chemically stable visible-light-driven photocatalyst, shows high activity for H_2 evolution as well as photocatalytic degradation of contaminants.[8−15] However, in a practical point of view, it should be noted that the photocatalytic activity of $ZnIn_2S_4$ still needs to be further improved. To further improve the H_2 evolution performance, many approaches have been proposed. For the visible-light-driven photocatalysts with proper band structures, the issue of photogenerated charge separation is a key factor strongly affecting the efficiency of the photocatalytic water-splitting process.[16−18] Clearly, in order to increase the utilization rate of the photogenerated charges and obtain high photocatalytic water-splitting activities, the photogenerated charges must be efficiently separated to avoid bulk/surface charge recombination and transfer to the separated active sites on the surface of the photocatalysts.[19−22] Recent studies have demonstrated that the charge separation and photocatalytic hydrogen-production activities were enhanced by selectively coupling $ZnIn_2S_4$ nanomaterials with other semiconductors (TiO_2, CdSe, ZnS, MoS_2, NiS, and so on) or noble metals (e.g., Pt).[23−28] Especially, carbon-based materials, such as active carbon, carbon nanotubes, and graphene, have been widely introduced due to their excellent conductivity and extraordinary chemical stability.[29−31] Among various nanostructured carbon materials, two-dimensional (2D) layered graphene and one-dimensional (1D) carbon material (carbon nanotubes and carbon nanofiber) have been promising materials. In study, apart from the random mixture of $ZnIn_2S_4$ and other semiconductors, lots of works have attempted to construct 1D and 2D nanocomposites by depositing functional inorganic nanomaterials on the carbon backbone. However, the relatively weak interaction between inorganic species and the carbon backbone usually leads to the

Received: May 26, 2014
Accepted: July 24, 2014
Published: July 24, 2014

   dx.doi.org/10.1021/am5032083 | ACS Appl. Mater. Interfaces 2014, 6, 13841−13849

dissatisfied uniformity and distribution of the inorganic component on the surface of the carbon backbone.[30−32] As a result, it is still highly desirable to design new strategies to fabricate well-defined structures by growing low-dimensional nanostructures of functional materials on the carbon backbone.

In the previous reports, in situ controlled growth approaches were developed to construct composites.[33−35] This kind of synthetic method can form effective interfacial contact and strong interaction between two components in the composite and lead to an enhanced photogenerated charge transfer and separation. Recently, the ultrathin structures, such as nanosheets, have been confirmed to show significantly improved photocatalytic activities by growing nanosheets on the supporter to form hierarchical structure composites basically due to the large specific surface areas and the enhanced photogenerated charge carrier transfer from the interior to the surface of photocatalysts to participate in the photocatalytic reactions.[24,35] Significant progress has been made in combining these advantages. For instance, Lou et al. prepared 1D hierarchical structures composed of Ni_3S_2 nanosheets on carbon nanotube backbones to significantly improve supercapacitors and photocatalytic H_2-production performance.[36] Among all the carbon materials, the electrochemical properties of 1D carbon nanofibers (CNFs) and carbon nanotubes are similar, but the carbon nanofibers can be easily prepared by electrospinning technology, more consistent with the requirement of a low cost compared to the carbon nanotubes.[37−44] To the best of our knowledge, there is no investigation focused on the CNFs@$ZnIn_2S_4$ composites for photocatalytic H_2 production.

In this work, we report on a simple technique based on a combination of electrospinning and solvothermal process to in situ grow $ZnIn_2S_4$ nanosheets on the carbon nanofiber backbone to form hierarchical core−shell CNFs@$ZnIn_2S_4$ composites. First, a 1D carbon nanofiber was prepared by electrospinning and subsequent calcination under a nitrogen atmosphere. Then, the as-prepared carbon nanofiber was used as an excellent supporting matrix for in situ growth of $ZnIn_2S_4$ nanosheets. The in situ growth process can help to form intimate contacts between $ZnIn_2S_4$ nanosheets and the carbon nanofiber backbone compared with the physical mixture, which helps the interfacial charge transfer driven by the excitation of $ZnIn_2S_4$ under visible-light irradiation and reduces the self-agglomeration. These synergistic effects made this composite system exhibit a significantly higher visible-light photocatalytic hydrogen evolution performance than those comprising a single component or a physical mixture of carbon nanofibers and $ZnIn_2S_4$.

2. EXPERIMENTAL SECTION

2.1. Preparation of Carbon Nanofibers (CNFs). The precursor solution (PAN, 8 wt %) was first prepared by mixing the polyacrylonitrile (PAN, molecular weight = 160 000) and solvent *N*,*N*-dimethylformamide (DMF, ≥99.9%) at 60 °C. The solution was spun into a nanofiber web through a positively charged capillary using an electrospinning apparatus at 10 kV. The negative electrode was connected to a drum winder collecting the nanofiber web. The electrospun nanofibers were collected as a web on an aluminum foil wrapped on the metal drum with a rotation speed of 300 rpm. The electrospun nanofiber web was stabilized in an air atmosphere at 250 °C for 1 h (heating rate was 1 °C min^{-1}) and then carbonized at 900 °C for 1 h in nitrogen at a ramp rate of 5 °C min^{-1}, and finally cooled to room temperature. Thus, carbon nanofibers (CNFs) were obtained.

2.2. Fabrication of Hierarchical Core−Shell CNFs@$ZnIn_2S_4$ Composites. In a typical procedure for the synthesis of hierarchical core−shell CNFs@$ZnIn_2S_4$ composites, the carbon nanofiber (the weight ratios of carbon nanofiber to $ZnIn_2S_4$ were 5, 10, 15, and 20 wt %) was dispersed into 15 mL of ethanol by ultrasonication for 30 min, respectively. Subsequently, 5 mL of glycerol, 0.3820 g of $In(NO_3)_3 \cdot 4.5H_2O$, 0.1110 g of $Zn(AC)_2 \cdot 6H_2O$, and 0.5272 g of L-cysteine hydrochloride monohydrate ($C_3H_7NO_2S \cdot HCl \cdot H_2O$) were added into the above solution under stirring for 20 min. Then, the obtained mixed solution was transferred to a 50 mL Teflon-lined stainless steel autoclave, which was heated to 180 °C and maintained for 24 h. After cooling to the room temperature, the as-synthesized solid products were rinsed several times using ethanol and dried at 70 °C for 12 h. For comparison, the blank $ZnIn_2S_4$ was prepared in the absence of carbon nanofibers using the same experimental conditions.

In order to determine the detailed content of carbon fibers in the CNFs@$ZnIn_2S_4$ composites, we added a certain amount of CNFs@$ZnIn_2S_4$ composites into diluted hydrochloric acid (3 mol L^{-1}) and stirred it overnight to ensure that $ZnIn_2S_4$ was dissolved completely. Then, the black suspension was filtered and washed with distilled water several times. Subsequently, the clear filtrate was diluted and determined by ICP-AES to get the concentration of Zn^{2+} and In^{3+}, so the contents of carbon fibers and $ZnIn_2S_4$ in the composite can be calculated, respectively. For the CNFs@$ZnIn_2S_4$ composites prepared using 5, 10, 15, and 20 wt % carbon nanofibers, the detected carbon fiber content is 5.23, 10.27, 15.35, and 20.47 wt %.

2.3. Characterization. The X-ray diffraction (XRD) of powder samples was examined by X-ray diffraction (XRD, Bruker D8 Advance diffractometer) monochromatized Cu Kα radiation (λ = 0.15418 nm). Transmission electron microscopy (TEM) and high-resolution TEM (HRTEM) images of samples were recorded in a JEOL 2100 microscope with a 200 kV accelerating voltage, along with scanning electron microscopy (SEM, Hitachi, S-4800). Photoluminescence (PL) spectra were measured at room temperature using a Fluoromax-4 Spectrophotometer (Horiba Jobin Yvon). The excitation wavelength was 300 nm, and the emission slit was 1.0 nm. The UV−visible diffuse reflectance spectra of the samples were obtained using a UV−visible spectrophotometer (Shimadzu UV-2550). The electrochemical impedance spectra (EIS) of the thin film made from these as-made materials were measured via a computer-controlled IM6e impedance measurement unit (Zahner Elektrik, Germany) in 0.25 M Na_2SO_3 and 0.35 M Na_2S aqueous solution under UV light and carried out by applying sinusoidal perturbations of 10 mV under a bias of −0.8 V, and the frequency ranges from 0.05 to 100 kHz. Zn^{2+} and In^{3+} concentrations of the samples were determined by inductively coupled plasma-atomic emission spectrometry (ICP-AES, Thermo ICAP6300).

2.4. Photocatalytic Hydrogen Production. The photocatalytic H_2 evolution from water was conducted in an online photocatalytic hydrogen production system (AuLight, Beijing, CEL-SPH2N). A powder sample of the catalyst (0.03 g) was suspended in a mixture of 100 mL of a mixed aqueous solution containing 0.35 M Na_2S and 0.25 M Na_2SO_3. The reaction was carried out by irradiating the suspension with light from a 300 W Xe lamp (AuLight, CEL-HXF-300, Beijing) that was equipped with an optical filter (λ > 420 nm) to cut off the light in the ultraviolet region. Prior to the reaction, the mixture was deaerated by evacuation to remove O_2 and CO_2 dissolved in water. Gas evolution was observed only under photoirradiation, being analyzed by an online gas chromatograph (SP7800, TCD, molecular sieve 5 Å, N_2 carrier, Beijing Keruida Limited).

The determination of the apparent quantum efficiency (AQE) for hydrogen generation was performed using the same closed circulating system under illumination of a 300 W Xe lamp with a band-pass filter (420 nm) system. The light intensity was measured using a Si photodiode (oreal 91105 V). The total light intensity was 1.5 mW (420 nm). The irradiation area was around 7 cm^2. Apparent quantum efficiency (AQE) was calculated by the following equation.[45]

$$\mathrm{AQE} = \frac{2 \times \text{the number of evolved } H_2 \text{ molecules}}{\text{the number of incident photons}} \times 100\% \quad (1)$$

3. RESULTS AND DISCUSSION

3.1. Structure and Morphology. Figure 1 shows the X-ray diffraction (XRD) patterns of the CNFs@$ZnIn_2S_4$

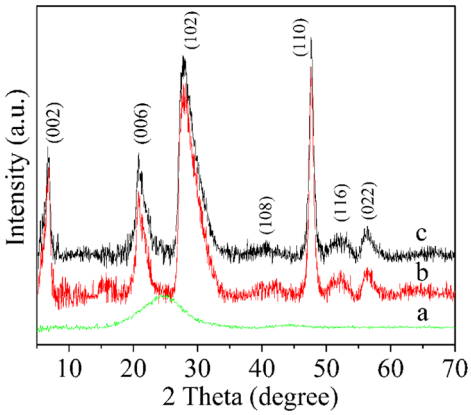

Figure 1. XRD patterns of carbon nanofibers (a), $ZnIn_2S_4$ (b), and hierarchical core−shell CNFs@$ZnIn_2S_4$ composites (15 wt % of CNFs) (c).

hierarchical heterostructures, $ZnIn_2S_4$, and pure carbon nanofibers. It can be found that the pure $ZnIn_2S_4$ shows the diffraction peaks of (002), (006), (102), and (110) crystal planes at 2θ = 6.5, 21.6, 27.8, and 47.2°, which can be indexed to a hexagonal phase of $ZnIn_2S_4$ (JCPDS No. 65-2023).[5,46] From the XRD pattern of the pure carbon nanofibers, it can be found that the broad peak is centered at around 25°, which is attributed to the (002) plane of the carbon structure in the carbon nanofibers.[47,48] All of the diffraction peaks of the CNFs@$ZnIn_2S_4$ composite can be indexed to the hexagonal $ZnIn_2S_4$. No cubic phase or impurity peaks can be detected from the XRD measurement. The XRD results revealed that carbon nanofibers did not affect the crystal phase of $ZnIn_2S_4$. However, no diffraction peaks corresponding to carbon nanofibers were observed in the XRD pattern of the CNFs@$ZnIn_2S_4$ composite, which was probably caused by its low crystallinity and low content. As an alternative approach, the Raman spectrum of the CNFs@$ZnIn_2S_4$ composite showed characteristic peaks that confirmed the appearance of carbon nanofibers (Figure S1, Supporting Information).

Figure 2A shows the SEM image of the as-prepared carbon nanofibers. The nanofibers have a diameter of about 150−200 nm and lengths of several tens of micrometers with a relative smooth surface. In comparison, Figure 2B shows the typical morphological characterizations of the hierarchical core−shell CNFs@$ZnIn_2S_4$ composites with a diameter of about 400−500 nm. It is easy to observe that the entire surface of the carbon nanofibers is fully decorated with uniform $ZnIn_2S_4$ nanosheets, which are evenly distributed across and connected to each other, forming a network of relief features on the surface of each carbon nanofiber. It can be estimated that the thickness of the $ZnIn_2S_4$ shell is about 125−175 nm. The TEM image of the CNFs@$ZnIn_2S_4$ composite in Figure 2C shows that $ZnIn_2S_4$ has a typical sheetlike structure and grows along the surface of carbon nanofibers. The corresponding high-resolution TEM image in Figure 2D shows a fringe spacing of 0.325 nm, which corresponds to the (102) plane of hexagonal phase $ZnIn_2S_4$.[5,49] Intimate junctions between $ZnIn_2S_4$ nanosheets and carbon nanofibers are indeed formed by the growth process. The in situ growth might provide an advantage in the formation of the intimate contact between $ZnIn_2S_4$ and the carbon nanofiber, which is crucial for forming an effective charge-separation nanojunction. Meanwhile, the HRTEM image of the CNFs@$ZnIn_2S_4$ hierarchical composite (Figure 2D) reveals that the thickness of $ZnIn_2S_4$ nanosheets grown on carbon nanofibers is significantly thin, and the nanosheets tend to bend and their edges are ragged as a result of minimizing the surface energy. For comparison, the blank $ZnIn_2S_4$ prepared in the absence of carbon nanofibers has a solid global morphology with a sheetlike surface (Figure S2, Supporting Information). The results suggest that the presence of carbon nanofibers can greatly inhibit the restacking of $ZnIn_2S_4$ during its nucleation

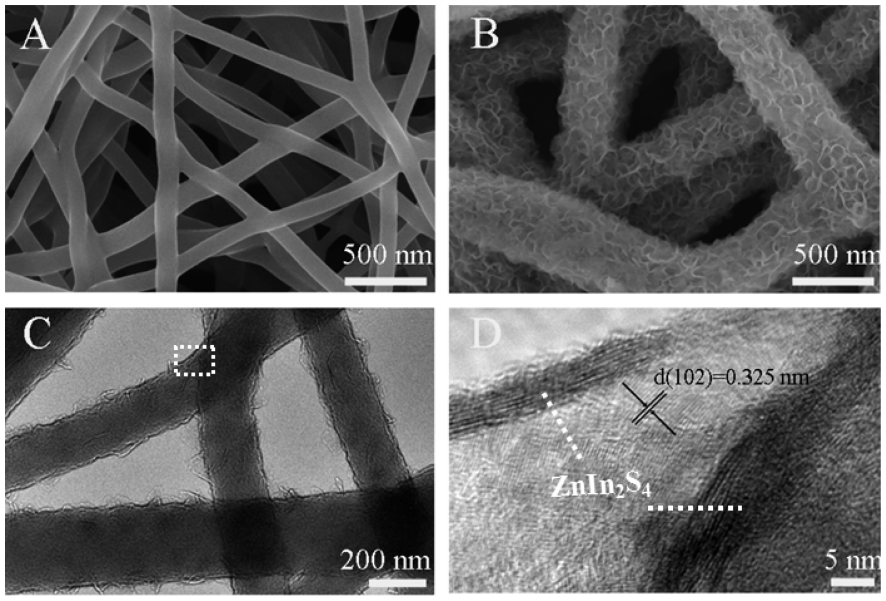

Figure 2. (A) SEM image of carbon nanofibers. (B) SEM image of hierarchical core−shell CNFs@$ZnIn_2S_4$ composite (15 wt % of CNFs). (C) Low-magnification TEM image of hierarchical core−shell CNFs@$ZnIn_2S_4$ composite (15 wt % of CNFs). (D) HRTEM image of the designated square part in (C).

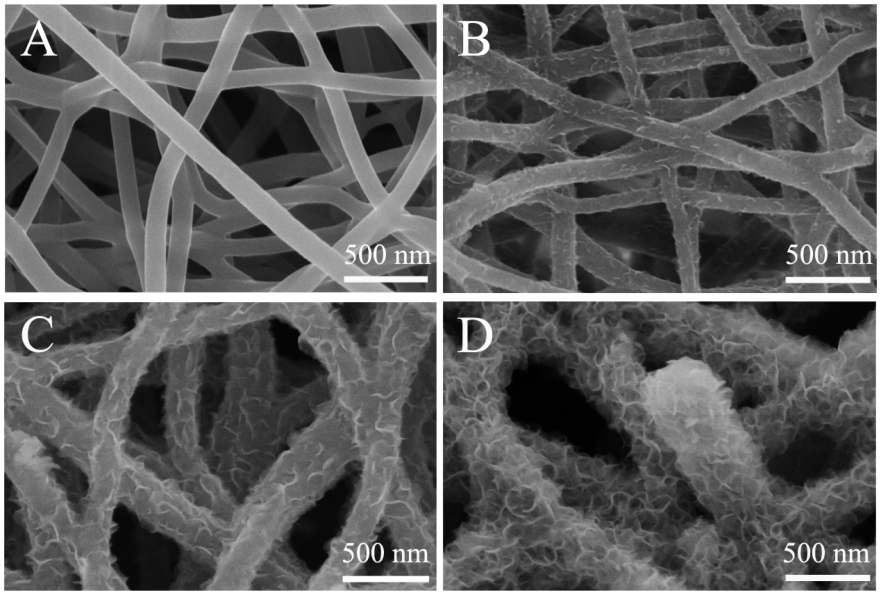

Figure 3. SEM images of the products obtained at different reaction times: 20 min (A), 1 h (B), 3 h (C), and 9 h (D).

and growth. It is reasonable to expect that these $ZnIn_2S_4$ nanosheets possess relatively high surface areas due to their thinner and two-dimensional morphologies.

To investigate the formation process of the hierarchical core−shell CNFs@$ZnIn_2S_4$ composites, samples prepared at different reaction times were collected and investigated by SEM. Compared to smooth surface of the original carbon nanofibers (Figure 3A), as shown in Figure 3B, at the early reaction stage (1 h), the surface of the carbon nanofibers became coarse and some nanoparticles (Figure 3B) appeared on the external surface of the carbon nanofibers through the initial nucleation reaction. It is mainly because the surface of carbon nanofibers can provide high energy nucleation sites for the nucleation and growth of $ZnIn_2S_4$ nanocrystals. When the reaction time was increased to 3 h, $ZnIn_2S_4$ nanoparticles growing on the surface of the carbon nanofibers changed significantly to $ZnIn_2S_4$ nanosheets (Figure 3C). By prolonging the reaction time, the number of the small nanosheets gradually increased, and finally the surfaces of the carbon nanofibers were uniformly covered by numerous nanosheets with cross-connections to each other (9 h, Figure 3D).

According to the results of time-dependent experiments, the formation process of the hierarchical core−shell CNFs@$ZnIn_2S_4$ composites can be elaborated in Scheme 1. First, carbon nanofibers were prepared via the electrospinning process. Then, the as-prepared carbon nanofibers were used as a supporting matrix to grow $ZnIn_2S_4$ nanosheets during the solvothermal process. For the carbon nanofiber, there are oxygen functional groups (e.g., hydroxyl) on its surface, which can be proved from the FTIR results in Figure S3 (Supporting Information). These functional groups act as anchor sites and can bind with Zn^{2+} and In^{3+} metal cations.[50] Meanwhile, the surface of carbon nanofibers can provide high energy nucleation sites for the nucleation and growth of $ZnIn_2S_4$ nanocrystals. During the solvothermal reaction, the anchored Zn^{2+} and In^{3+} metal cations can in situ react with the glycerol to form metal glycerolate complexes, which then further reacted with S^{2-} ions to form $ZnIn_2S_4$ nanocrystals.[33] Besides, the stacking force between $ZnIn_2S_4$ nuclei and basal planes of carbon nanofibers is also beneficial for the in situ formation of $ZnIn_2S_4$ nanocrystals

Scheme 1. Schematic Illustration of the Formation Process of the Hierarchical Core−Shell CNFs@$ZnIn_2S_4$ Composites[a]

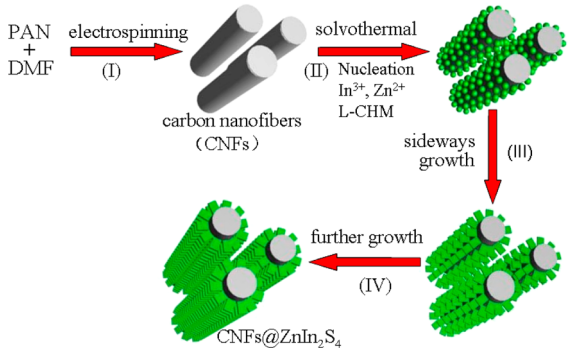

[a](I) Synthesis of carbon nanofibers by electrospinning, followed by thermal treatments; (II) in situ formation of $ZnIn_2S_4$ nanocrystal shell on carbon nanofibers; (III) chemical conversion of $ZnIn_2S_4$ nanocrystals into nanosheets; and (IV) further growth of $ZnIn_2S_4$ nanosheets to form CNFs@$ZnIn_2S_4$ hierarchical composites.

occurring on the surface of carbon nanofibers. As the reaction continued, the secondary nucleation was much more preferential on the $ZnIn_2S_4$ nuclei surface than those in the solution. Subsequently, these nanocrystals then continued to grow sideways, which led to the formation of ultrathin curled nanosheets on the carbon nanofibers' surface.[7] Finally, the $ZnIn_2S_4$ nanosheets grew larger and more densely along with the surface of carbon nanofibers (Figure 3C,D) with the increase of the reaction time.

In photocatalytic study, for the composite photocatalyst where one component is deposited on the surface of the other one, it is important to control the coverage because both complete and sparse coverage of one component on the other will reduce the catalytic efficiency. In this study, in order to obtain a more efficient photocatalytic catalyst, we adjusted the ratio of carbon nanofibers in the hierarchical core−shell CNFs@$ZnIn_2S_4$ composites. When the content of carbon nanofibers was high, there are small amounts of $ZnIn_2S_4$

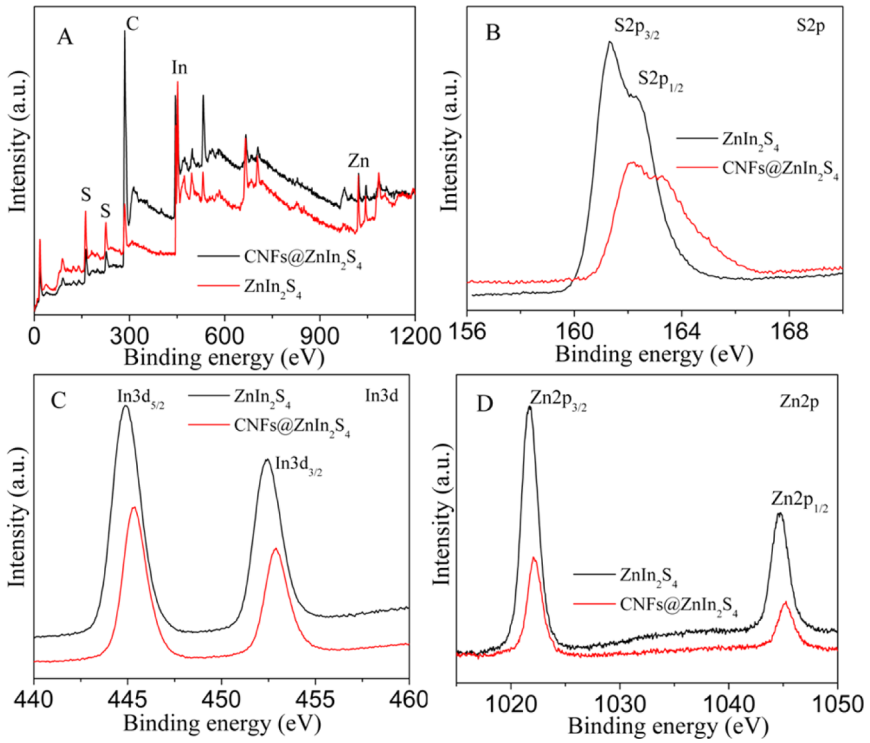

Figure 4. XPS spectra of the as-obtained hierarchical core−shell CNFs@$ZnIn_2S_4$ composite (15 wt % of CNFs) and $ZnIn_2S_4$: Survey XPS spectra (A) and high-resolution spectra of S 2p (B), In 3d (C), and Zn 2p (D), respectively.

nanosheets on the surface of the carbon nanofibers (Figure S4A, Supporting Information), indicating that high coverage of nanosheets needed a sufficient amount of $ZnIn_2S_4$. Obviously, without adequate fluffy nanosheets on the surface, the multiple light reflections and light-harvesting would be reduced in the composite and thus decrease the quantity of photogenerated electrons and holes. However, minute carbon nanofibers would make excess $ZnIn_2S_4$ nanosheets assemble to form $ZnIn_2S_4$ microspheres (Figure S4B, Supporting Information).

3.2. Spectra Analysis. X-ray photoelectron spectroscopy (XPS) was used to investigate the chemical states of different elements in the hierarchical core−shell CNFs@$ZnIn_2S_4$ composite (15 wt % of CNFs). In the composites, the values of S $2p_{1/2}$ and S $2p_{3/2}$ peaks (Figure 4B) corresponding to $ZnIn_2S_4$ are also slightly lower than those of pure $ZnIn_2S_4$ (162.6 and 161.6 eV).[51] Meanwhile, the In 3d and Zn 2p were also examined (Figure 4C,D). The binding energies of Zn 2p (1021.8 and 1044.6 eV) and In 3d (444.9 and 452.4 eV) for the hierarchical core−shell CNFs@$ZnIn_2S_4$ composite are slightly higher than those of pure $ZnIn_2S_4$.[15] Such a shift to high binding energy suggests a strong interaction between $ZnIn_2S_4$ and the carbon nanofibers, which was beneficial to the transfer of photogenerated electrons during the photocatalysis.[18,46] It is believed that, when $ZnIn_2S_4$ are connected to carbon nanofibers, the electron transfer from $ZnIn_2S_4$ to the more electronegative carbon nanofibers may result in a decrease of the electron density of Zn^{2+} and In^{3+}.[28] Therefore, the binding energies of Zn 2p and In 3d shift to a high binding energy in CNFs@$ZnIn_2S_4$ composite.

Figure 5 shows the diffuse reflectance spectra of the hierarchical core−shell CNFs@$ZnIn_2S_4$ composites with different carbon nanofiber contents and pure $ZnIn_2S_4$. As can be seen, the pure $ZnIn_2S_4$ shows photoabsorption properties from the UV light region to the visible-light region. Notably, for the

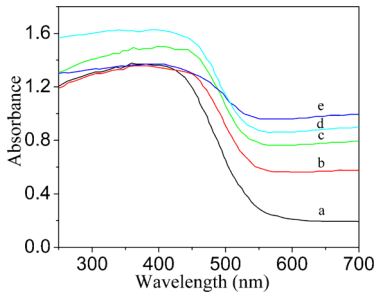

Figure 5. UV−vis diffuse reflectance absorption spectra (DRS) of $ZnIn_2S_4$ (a) and hierarchical core−shell CNFs@$ZnIn_2S_4$ composites with different carbon nanofiber contents: (b) 5, (c) 10, (d) 15, (e) 20 wt %.

CNFs@$ZnIn_2S_4$ hierarchical composites, significant enhancement of light absorption in the visible-light region (>400 nm) can be seen, which can be mainly attributed to carbon itself absorbing visible light.[52] Moreover, with increasing black carbon nanofiber content, the visible-light absorption also increased.

As is known, photocatalytic activity is dependent on the trapping and lifetime of photogenerated electrons and holes in the semiconductor catalyst. Photoluminescence (PL) emission spectra are often employed to study surface structure and excited states, and it can provide useful information about the efficiency of charge carrier trapping and recombination in semiconductor particles since the PL emission comes from the recombination of free charge carriers.[53,54] In this study, the PL spectrum (Figure 6, spectra a) of $ZnIn_2S_4$ shows a broad peak around 560 nm, which attributed to the emission of the band-gap transition with the energy of light approximately equal to the band-gap energy of $ZnIn_2S_4$ (550 nm).[27] For the hierarchical core−shell CNFs@$ZnIn_2S_4$ composites, the PL

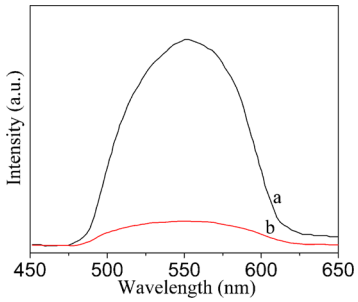

Figure 6. Photoluminescence spectra of pristine $ZnIn_2S_4$ (a) and hierarchical core–shell CNFs@$ZnIn_2S_4$ composite (15 wt % of CNFs) (b).

spectrum (Figure 6, spectrum b) is similar to that of pure $ZnIn_2S_4$. However, a significant fluorescence decrease (or quenching) was observed, indicating a reduced charge recombination in comparison to $ZnIn_2S_4$ alone. The results of PL spectra proved that the introduction of carbon nanofibers in the composites can improve the separation of electron–hole pairs under visible-light irradiation due to their excellent electron-accepting and electron-transport properties similar to those of carbon nanotubes, which can provide a convenient way to direct the flow of photogenerated charge carriers and increase the life of electron–hole pairs generated by semiconductors under light irradiation.

3.3. Electrochemical Impedance Analysis. Electrochemical impedance spectroscopy (EIS) is a powerful tool in studying the charge transfer process occurring in the three-electrode system,[55] and the EIS Nyquist plots of the two samples are shown in Figure 7. As has been reported, the

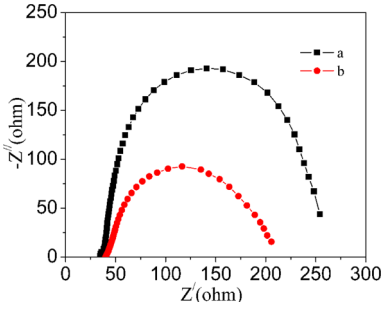

Figure 7. Nyquist plots of (a) $ZnIn_2S_4$ and (b) hierarchical core–shell CNFs@$ZnIn_2S_4$ composite (15 wt % of CNFs) electrodes in aqueous solution containing 0.25 M Na_2SO_3/0.35 M Na_2S under visible-light irradiation.

intermediate-frequency response is associated with the electron transport and transfer at the $ZnIn_2S_4$/electrode interface.[56] The hierarchical core–shell CNFs@$ZnIn_2S_4$ composite shows a smaller semicircle in the middle-frequency region in comparison to the $ZnIn_2S_4$, which indicates the fastest interfacial charge transfer.[57,58] Therefore, it can be proved that the introduction of carbon nanofibers can improve the interfacial charge transfer and separation in the hierarchical core–shell CNFs@$ZnIn_2S_4$ composite system and thus lower the charge recombination because of the formation of a junction between carbon nanofibers and $ZnIn_2S_4$. Overall, carbon nanofibers can act as both a $ZnIn_2S_4$ nanosheet substrate and an electron collector and transporter in the composite. This can contribute to the improvement of the photocatalytic H_2-production activity.

3.4. Photocatalytic H_2 Evolution Property. The photocatalytic performances of the as-prepared hierarchical core–shell CNFs@$ZnIn_2S_4$ composites were monitored for hydrogen evolution from the aqueous solution containing 0.25 M Na_2SO_3/0.35 M Na_2S as sacrificial reagents under visible-light irradiation. In order to reveal the possible synergetic effect of the hybrid structure, the control experiments of photocatalytic H_2 production with $ZnIn_2S_4$ alone and carbon nanofibers alone have been also performed. As shown in Figure 8A, the bare

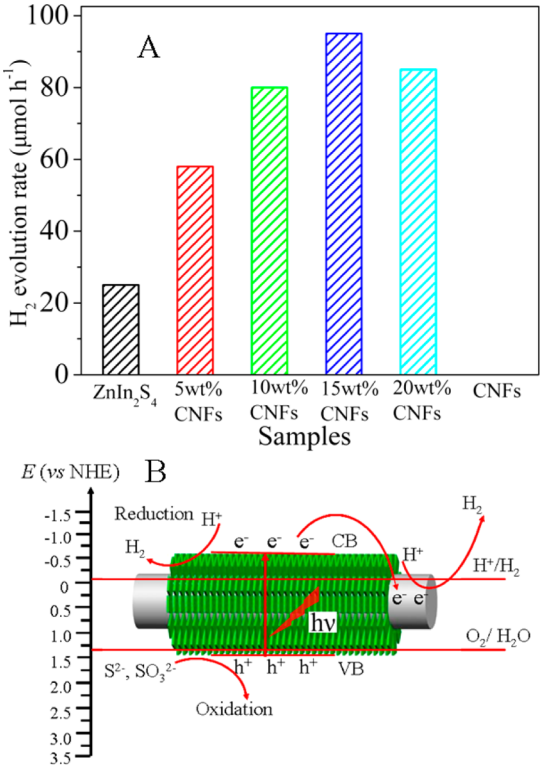

Figure 8. (A) Comparison of the photocatalytic H_2 evolution rate of $ZnIn_2S_4$, carbon nanofibers (CNFs), and the hierarchical core–shell CNFs@$ZnIn_2S_4$ composites with different carbon nanofiber (CNF) contents. (B) The proposed photocatalytic H_2 evolution mechanism for the hierarchical core–shell CNFs@$ZnIn_2S_4$ composites.

$ZnIn_2S_4$ shows acceptable H_2 evolution properties (24 μmol h^{-1}), which are ascribed to its appropriate band gap and crystal structure. The carbon nanofibers exhibited no photocatalytic hydrogen evolution performance under visible-light irradiation. The result showed that a carbon nanofiber is not a photocatalyst, but the hierarchical core–shell CNFs@$ZnIn_2S_4$ composites exhibited significantly enhanced the photocatalytic activity, highlighting the usefulness of the combination with 1D carbon nanofibers in improving the photocatalytic activity of the $ZnIn_2S_4$ nanosheets. This excellent H_2-production performance of the hierarchical core–shell CNFs@$ZnIn_2S_4$ composites can be ascribed to several factors. First, fast separation of the photoinduced electron/hole pairs plays an important role. The intimate contact and formation of junctions between $ZnIn_2S_4$ and carbon nanofibers could offer effective charge separation, and meanwhile, the 1D geometrical character of carbon nanofibers in the hierarchical structure composites acts as the electron acceptor and makes electron transport excellent.[24] The

improved charge-separation rate was proved by the results of PL (Figure 6) and EIS (Figure 7) measurements. Second, carbon nanofibers may serve as a good photosensitizer, which would enhance the visible-light absorption for the composite photocatalyst.[36] In addition, the unique hierarchical structure should also be related to the enhanced photocatalytic activity. The exposure of a large external surface area of the thin $ZnIn_2S_4$ nanosheets attached onto the carbon nanofiber backbone could also offer much higher catalytic reaction efficiency than the aggregated $ZnIn_2S_4$ microspheres owing to the increased reaction active sites and the electron-tunneling effect through the $ZnIn_2S_4$ thin nanosheets to carbon nanofibers.

The expected working mechanism for photocatalytic H_2 evolution over the hierarchical core−shell CNFs@$ZnIn_2S_4$ composites under visible-light irradiation is shown in Figure 8B. Under visible-light irradiation, the photogenerated electrons are excited from the valence band (VB) to the conduction band (CB) of $ZnIn_2S_4$. Meanwhile, the carbon nanofibers incorporated into the 1D hierarchical structure act as the electron acceptor and the photoexcited electrons in the conduction band of $ZnIn_2S_4$ can quickly transfer to the carbon nanofibers and transport freely along the cylindrical nanostructure, which would ensure efficient charge transfer and at the same time retard the charge recombination. The remaining photogenerated electrons are accessible to the adsorbed H^+ ions (from water ionization) to produce H_2. Meanwhile, the sacrificial reagent will complement the electrons to the remaining holes in the valence band of $ZnIn_2S_4$. This process greatly enhanced the separation ability of the photoexcited electrons and holes. Furthermore, the amount of carbon nanofibers is an important factor affecting the photocatalytic activity. When the carbon nanofiber content is low in the composite, the photocatalytic activity of the composite is relatively low. It is mainly because the thickness of the $ZnIn_2S_4$ shell is relatively thick, and meanwhile, excess $ZnIn_2S_4$ nanosheets assemble to form $ZnIn_2S_4$ microspheres, which would separate from the carbon nanofibers. Therefore, only a small amount of junctions can form between $ZnIn_2S_4$ and the carbon nanofiber. With the increase of carbon nanofiber content in the composite, the rate of H_2 evolution is at first increased and then decreased. The optimum amount of carbon nanofibers is ca. 15 wt %. On this condition, the obtained CNFs@$ZnIn_2S_4$ composite has a proper $ZnIn_2S_4$ shell thickness and shows the highest H_2 production (95 μmol h^{-1}). The apparent quantum efficiency (AQE) of the CNFs@$ZnIn_2S_4$ composite (15 wt % of CNFs) is 25.35% at 420 nm, which is higher than that (8.15%) of the pure $ZnIn_2S_4$. Moreover, the apparent quantum efficiency (AQE) of the CNFs@$ZnIn_2S_4$ composite is 18.15% and 2.04% at 450 and 500 nm, respectively. The apparent quantum efficiency decreases with increasing the incident light wavelength, which is consistent with the change tendency of the DRS spectrum (Figure 5). While further increasing the carbon nanofiber amount (20 wt %), the H_2-production rate gradually decreased. The reason is likely due to the shading effect.[25,36,59] Because the thickness of the $ZnIn_2S_4$ shell gradually becomes thin, the carbon nanofiber in the composites should increase the opacity, leading to a decrease of light absorption passing through the reaction suspension solution.

Meanwhile, a detailed investigation of the influence of the coupling effect between $ZnIn_2S_4$ and a carbon nanofiber on the photocatalytic activity was done to give an insight into the structure−property−performance relationship of such composites. For comparison, another sample, the physical mixture of $ZnIn_2S_4$ and carbon nanofibers (15 wt %), was also used for H_2 evolution under the same condition (Figure S5, Supporting Information). Apparently, the hierarchical core−shell CNFs@$ZnIn_2S_4$ composites showed considerably enhanced H_2 evolution activity. It indicates that the strong coupling effect between $ZnIn_2S_4$ nanosheets and carbon nanofibers is awfully important for the photogenerated charge transfer. When $ZnIn_2S_4$ nanosheets are grown on the surface of carbon nanofibers, the formed hierarchical composite structure makes the photogenerated electrons easily transfer to the carbon nanofiber, leading to efficient separation and prolonged recombination time of electron−hole pairs, which is confirmed by the results of PL and EIS measurements (Figures 6 and 7). Meanwhile, because $ZnIn_2S_4$ nanosheets are uniformly grown on the surface of carbon nanofibers, excessive aggregation of $ZnIn_2S_4$ can be avoided, which will increase reaction active sites and reactant adsorption.[57]

In addition to photocatalytic activity, for a photocatalyst to be commercially viable, the stability is another important issue for their practical applications. As shown in Figure S6 (Supporting Information), the H_2 evolution performance of $ZnIn_2S_4$ showed some reduction after the fourth recycle experiment. However, the hierarchical core−shell CNFs@$ZnIn_2S_4$ composite showed significant stability for H_2 generation by performing the recycle experiments under the same conditions. It is because the intimate contact between $ZnIn_2S_4$ nanosheets and carbon nanofibers in the hierarchical core−shell CNFs@$ZnIn_2S_4$ composite favors the vectorial transfer of the photogenerated electrons from the conduction band of $ZnIn_2S_4$ to the carbon nanofibers. This space separation is beneficial in preventing the reduction of In^{3+} and Zn^{2+}, which further increases the stability of $ZnIn_2S_4$.[33]

4. CONCLUSIONS

In summary, hierarchical core−shell CNFs@$ZnIn_2S_4$composites were synthesized through a facile two-step approach involving electrospinning and a subsequent solvothermal process. This method affords an effective route to make $ZnIn_2S_4$ nanosheets grow well on the surface of carbon nanofibers with a strong coupling effect. The obtained $ZnIn_2S_4$ nanosheets were well dispersed on the surface of carbon nanofibers. The photocatalytic H_2 evolution performance of the as-synthesized hierarchical core−shell CNFs@$ZnIn_2S_4$ composite is significantly higher than that of $ZnIn_2S_4$ alone. The enhanced photocatalytic H_2 evolution properties could be attributed to the synergetic catalytic effect of $ZnIn_2S_4$ nanosheets and carbon nanofibers in the composites. The strong interaction benefiting from the coupling effect between carbon nanofibers and $ZnIn_2S_4$ nanosheets can effectively prohibit the recombination of photogenerated electron−hole pairs. It was expected that the hierarchical core−shell CNFs@$ZnIn_2S_4$ composites could have great potential for practical application in photocatalysis and photoelectrochemistry.

■ ASSOCIATED CONTENT

Supporting Information

Raman spectrum of the hierarchical core−shell CNFs@$ZnIn_2S_4$ composite, SEM images of $ZnIn_2S_4$ and the hierarchical core−shell CNFs@$ZnIn_2S_4$ composite products obtained from different carbon nanofiber contents, the comparison of the photocatalytic H_2 evolution rate of the hierarchical core−shell CNFs@$ZnIn_2S_4$ composite (15 wt %, of CNFs) and the

physical mixture of $ZnIn_2S_4$ and carbon nanofiber (15 wt %), and FT-IR spectrum of carbon nanofiber. This material is available free of charge via the Internet at http://pubs.acs.org.

AUTHOR INFORMATION

Corresponding Authors

*E-mail: tiangh@hlju.edu.cn. Tel: +86 451 8660 4330. Fax: +86 451 8667 3647 (G.T.).

*E-mail: fuhg@vip.sina.com (H.F.).

Notes

The authors declare no competing financial interest.

ACKNOWLEDGMENTS

We gratefully acknowledge the support of this research by the Key Program Projects of the National Natural Science Foundation of China (No. 21031001), the National Natural Science Foundation of China (51272070, 91122018, 20971040, 21371053), the Cultivation Fund of the Key Scientific and Technical Innovation Project, Ministry of Education of China (No. 708029), the Program for Innovative Research Team in University (IRT-1237), the Natural Science Foundation of Heilongjiang Province of China (E201455), and the Special Research Fund for the Doctoral Program of Higher Education of China (20112301110002).

REFERENCES

(1) Ha, J. W.; Ruberu, T. P. A.; Han, R.; Dong, B.; Vela, J.; Fang, N. Super-Resolution Mapping of Photogenerated Electron and Hole Separation in Single Metal−Semiconductor Nanocatalysts. *J. Am. Chem. Soc.* **2014**, *136*, 1398−1408.

(2) Gratzel, M. Photoelectrochemical Cells. *Nature* **2001**, *414*, 338−344.

(3) Cho, I. S.; Chen, Z.; Forman, A. J.; Kim, D. R.; Rao, P. M.; Jaramillo, T. F.; Zheng, X. Branched TiO_2 Nanorods for Photoelectrochemical Hydrogen Production. *Nano Lett.* **2011**, *11*, 4978−4984.

(4) Hou, J. G.; Yang, C.; Wang, Z.; Jiao, S. Q.; Zhu, H. M. Hydrothermal Synthesis of $CdS/CdLa_2S_4$ Heterostructures for Efficient Visible-Light-Driven Photocatalytic Hydrogen Production. *RSC Adv.* **2012**, *2*, 10330−10336.

(5) Mei, Z. W.; Ouyang, S. X.; Tang, D. M.; Kako, T.; Golberg, D.; Ye, J. H. An Ion-Exchange Route for the Synthesis of Hierarchical $In_2S_3/ZnIn_2S_4$ Bulk Composite and Its Photocatalytic Activity under Visible-Light Irradiation. *Dalton Trans.* **2013**, *42*, 2687−2690.

(6) Shen, Z. Y.; Chen, G.; Wang, Q.; Yu, Y. G.; Zhou, C.; Wang, Y. Sonochemistry Synthesis and Enhanced Photocatalytic H_2-Production Activity of Nanocrystal Sembedded in $CdS/ZnS/In_2S_3$ Microspheres. *Nanoscale* **2012**, *4*, 2010−2017.

(7) Zhang, K.; Guo, L. J. Metal Sulphide Semiconductors for Photocatalytic Hydrogen Production. *Catal. Sci. Technol.* **2013**, *3*, 1672−1690.

(8) Chaudhari, N. S.; Warule, S. S.; Kale, B. B. Architecture of Rose and Hollow Marigold-like $ZnIn_2S_4$ Flowers: Structural, Optical and Photocatalytic Study. *RSC Adv.* **2014**, *4*, 12182−12187.

(9) Li, F.; Chen, G. P.; Luo, J. H.; Huang, Q. L.; Luo, Y. H.; Meng, Q. B.; Li, D. M. Band Engineering of Cu^{2+} Doped $In_{2x}Zn_{3(1-x)}S_3$ Solid Solution with High Photocatalytic Activity for H_2 Production under Visible Light. *Catal. Sci. Technol.* **2013**, *3*, 1993−1999.

(10) Shen, S. H.; Zhao, L.; Guo, L. J. $Zn_mIn_2S_{3+m}$ (m = 1−5, Integer): A New Series of Visible-Light-Driven Photocatalysts for Splitting Water to Hydrogen. *Int. J. Hydrogen Energy.* **2010**, *35*, 10148−10154.

(11) Chen, Z. X.; Li, D. Z.; Zhang, W. J.; Chen, C.; Li, W. J.; Sun, M.; He, Y. H.; Fu, X. Z. Low-Temperature and Template-Free Synthesis of $ZnIn_2S_4$ Microspheres. *Inorg. Chem.* **2008**, *47*, 9766−9772.

(12) Shang, L.; Zhou, C.; Bian, T.; Yu, H. J.; Wu, L. Z.; Tung, C. H.; Zhang, T. R. Facile Synthesis of Hierarchical $ZnIn_2S_4$ Submicrospheres Composed of Ultrathin Mesoporous Nanosheets as a highly Efficient Visible-Light-Driven Photocatalyst for H_2 Production. *J. Mater. Chem. A* **2013**, *1*, 4552−4558.

(13) Xu, Z. D.; Li, Y. X.; Peng, S. Q.; Lu, G. X.; Li, S. B. Composition, Morphology and Photocatalytic Activity of Zn-In-S Composite Synthesized by a NaCl-Assisted Hydrothermal Method. *CrystEngComm* **2011**, *13*, 4770−4776.

(14) Chen, Y. J.; Hu, S. W.; Liu, W. J.; Chen, X. Y.; Wu, L.; Wang, X. X.; Liu, P.; Li, Z. H. Controlled Syntheses of Cubic and Hexagonal $ZnIn_2S_4$ Nanostructures with Different Visible-Light Photocatalytic Performance. *Dalton Trans.* **2011**, *40*, 2607−2613.

(15) Xu, Z. D.; Li, Y. X.; Peng, S. Q.; Lu, G. X.; Li, S. B. NaCl-Assisted Low Temperature Synthesis of Layered Zn-In-S photocatalyst with High Visible-Light Activity for Hydrogen Evolution. *RSC Adv.* **2012**, *2*, 3458−3466.

(16) Chen, Z. X.; Li, D. Z.; Zhang, W. J.; Shao, Y.; Chen, T. W.; Sun, M.; Fu, X. Z. Photocatalytic Degradation of Dyes by $ZnIn_2S_4$ Microspheres under Visible Light Irradiation. *J. Phys. Chem. C* **2009**, *113*, 4433−4440.

(17) Lei, Z. B.; You, W. S.; Liu, M. Y.; Zhou, G. H.; Takata, T.; Hara, M.; Domen, K.; Li, C. Photocatalytic Water Reduction under Visible Light on a Novel $ZnIn_2S_4$ Catalyst Synthesized by Hydrothermal Method. *Chem. Commun.* **2003**, 2142−2143.

(18) Peng, S. J.; Li, L. L.; Wu, Y. Z.; Jia, L.; Tian, L. L.; Srinivasan, M.; Ramakrishna, S.; Yan, Q. Y.; Mhaisalkar, S. G. Size- and Shape-Controlled Synthesis of $ZnIn_2S_4$ Nanocrystals with High Photocatalytic Performance. *CrystEngComm* **2013**, *15*, 1922−1930.

(19) Li, H. F.; Yu, H. T.; Chen, S.; Zhao, H. M.; Zhang, Y. B.; Quan, X. Fabrication of Graphene Wrapped $ZnIn_2S_4$ Microspheres Heterojunction with Enhanced Interfacial Contact and Its Improved Photocatalytic Performance. *Dalton Trans.* **2014**, *43*, 2888−2894.

(20) Peng, S. J.; Zhu, P. N.; Mhaisalkar, S. G.; Ramakrishna, S. Self-Supporting Three-Dimensional $ZnIn_2S_4$/PVDF−Poly(MMA-*co*-MAA) Composite Mats with Hierarchical Nanostructures for High Photocatalytic Activity. *J. Phys. Chem. C* **2012**, *116*, 13849−13857.

(21) Gao, B.; Liu, L. F.; Liu, J. D.; Yang, F. L. Photocatalytic Degradation of 2,4,6-Tribromophenol over Fe-Doped $ZnIn_2S_4$: Stable Activity and Enhanced Debromination. *Appl. Catal., B* **2013**, *129*, 89−97.

(22) Fang, F.; Chen, L.; Chen, Y. B.; Wu, L. M. Synthesis and Photocatalysis of $ZnIn_2S_4$ Nano/Micropeony. *J. Phys. Chem. C* **2010**, *114*, 2393−2397.

(23) Xu, B.; He, P. L.; Liu, H. L.; Wang, P. P.; Zhou, G.; Wang, X. A 1D/2D Helical $CdS/ZnIn_2S_4$ Nano-Heterostructure. *Angew. Chem., Int. Ed.* **2014**, *53*, 2339−2343.

(24) Li, Y. X.; Wang, J. X.; Peng, S. Q.; Lu, G. X.; Li, S. B. Photocatalytic Hydrogen Generation in the Presence of Glucose over ZnS-Coated $ZnIn_2S_4$ under Visible Light Irradiation. *Int. J. Hydrogen Energy* **2010**, *35*, 7116−7126.

(25) Chai, B.; Peng, T. Y.; Zeng, P.; Zhang, X. H. Preparation of a MWCNTs/$ZnIn_2S_4$ Composite and Its Enhanced Photocatalytic Hydrogen Production under Visible-Light Irradiation. *Dalton Trans.* **2012**, *41*, 1179−1186.

(26) Hou, J. G.; Yang, C.; Cheng, H. J.; Wang, Z.; Jiao, S. Q.; Zhu, H. M. Ternary 3D Architectures of CdS QDs/Graphene/$ZnIn_2S_4$ Heterostructures for Efficient Photocatalytic H_2 Production. *Phys. Chem. Chem. Phys.* **2013**, *15*, 15660−15668.

(27) Wei, L.; Chen, Y. J.; Lin, Y. P.; Wu, H. S.; Yuan, R. S.; Li, Z. H. MoS_2 as Non-Noble-Metal Co-catalyst for Photocatalytic Hydrogenevolution over Hexagonal $ZnIn_2S_4$ under Visible Light Irradiations. *Appl. Catal., B* **2014**, *144*, 521−527.

(28) Wei, L.; Chen, Y.; Zhao, J.; Li, Z. Preparation of NiS/$ZnIn_2S_4$ as a Superior Photocatalyst for Hydrogen Evolution under Visible Light Irradiation. *Beilstein J. Nanotechnol.* **2013**, *4*, 949−955.

(29) Chen, Y. J.; Ge, H.; Wei, L.; Li, Z. H.; Yuan, R. S.; Ping Liu, P.; Fu, X. Z. Reduction Degree of Reduced Graphene Oxide (RGO) Dependence of Photocatalytic Hydrogen Evolution Performance over RGO/$ZnIn_2S_4$ Nanocomposites. *Catal. Sci. Technol.* **2013**, *3*, 1712−1717.

(30) Kongkanand, A.; Dominguez, R. M.; Kamat, P. V. Single Wall Carbon Nanotube Scaffolds for Photoelectrochemical Solar Cells. Capture and Transport of Photogenerated Electrons. *Nano Lett.* **2007**, *7*, 676−680.
(31) Vietmeyer, F.; Seger, B.; Kamat, P. V. Anchoring ZnO Particles on Functionalized Single Wall Carbon Nanotubes. Excited State Interactions and Charge Collection. *Adv. Mater.* **2007**, *19*, 2935−2940.
(32) Wen, Z. H.; Wang, Q.; Zhang, Q.; Li, J. H. In Situ Growth of Mesoporous SnO_2 on the Multiwalled Carbon Nanotubes: A Novel Composite with Porous-Tube Structure as Anode for Lithium Batteries. *Adv. Funct. Mater.* **2007**, *17*, 2772−2778.
(33) Zhou, J.; Tian, G. H.; Chen, Y. J.; Meng, X. Y.; Shi, Y. H.; Cao, X. R.; Pan, K.; Fu, H. G. *In Situ* Controlled Growth of $ZnIn_2S_4$ Nanosheets on Reduced Graphene Oxide for Enhanced Photocatalytic Hydrogen Production Performance. *Chem. Commun.* **2013**, *49*, 2237−2239.
(34) Ye, L.; Fu, J. L.; Xu, Z.; Yuan, R. S.; Li, Z. H. Facile One-Pot Solvothermal Method to Synthesize Sheet-on-Sheet Reduced Graphene Oxide (RGO)/$ZnIn_2S_4$ Nanocomposites with Superior Photocatalytic Performance. *ACS. Appl. Mater. Interfaces* **2014**, *6*, 3483−3490.
(35) Tian, G. H.; Chen, Y. J.; Zhou, J.; Tian, G. H.; Li, R.; Wang, C. J.; Fu, H. G. *In Situ* Growth of Bi_2MoO_6 on Reduced Graphene Oxide Nanosheets for Improved Visible-Light Photocatalytic Activity. *CrystEngComm* **2014**, *16*, 842−849.
(36) Zhu, T.; Bin Wu, H. B.; Wang, Y. B.; Xu, R.; Lou, X. W. Formation of 1D Hierarchical Structures Composed of Ni_3S_2 Nanosheets on CNTs Backbone for Supercapacitors and Photocatalytic H_2 Production. *Adv. Energy Mater.* **2012**, *2*, 1497−1502.
(37) Xu, D. D.; Xu, Q.; Wang, K. X.; Chen, J.; Chen, Z. M. Fabrication of Free-Standing Hierarchical Carbon Nanofiber/Graphene Oxide/Polyaniline Films for Supercapacitors. *ACS Appl. Mater. Interfaces* **2014**, *6*, 200−209.
(38) Chen, L. F.; Zhang, X. D.; Liang, H. W.; Kong, M. G.; Guan, Q. F.; Chen, P.; Wu, Z. Y.; Yu, S. H. Synthesis of Nitrogen-Doped Porous Carbon Nanofibers as an Efficient Electrode Material for Supercapacitors. *ACS Nano* **2012**, *6*, 7092−7102.
(39) Arshad, S. N.; Naraghi, M.; Chasiotis, I. Strong Carbon Nanofibers from Electrospun Polyacrylonitrile. *Carbon* **2011**, *49*, 1710−1719.
(40) Liu, J.; Yue, Z.; Fong, H. Continuous Nanoscale Carbon Fibers with Superior Mechanical Strength. *Small* **2009**, *5*, 536−542.
(41) Zou, G.; Zhang, D.; Dong, C.; Li, H.; Xiong, K.; Fei, L.; Qian, Y. Carbon Nanofibers: Synthesis, Characterization, and Electrochemical Properties. *Carbon* **2006**, *44*, 828−832.
(42) Lallave, M.; Bedia, J.; Ruiz-Rosas, R.; Rodriguez-Mirasol, J.; Cordero, T.; Otero, J. C.; Marquez, M.; Barrero, A.; Loscertales, I. G. Filled and Hollow Carbon Nanofibers by Coaxial Electrospinning of Alcell Lignin without Binder Polymers. *Adv. Mater.* **2007**, *19*, 4292−4296.
(43) Zhou, Z.; Lai, C.; Zhang, L.; Qian, Y.; Hou, H.; Reneker, D. H.; Fong, H. Development of Carbon Nanofibers from Aligned Electrospun Polyacrylonitrile Nanofiber Bundles and Characterization of Their Microstructural, Electrical, and Mechanical Properties. *Polymer* **2009**, *50*, 2999−3006.
(44) He, Y. M.; Chen, W. J.; Zhou, J. Y.; Li, X. D.; Tang, P. Y.; Zhang, Z. X.; Fu, J. C.; Xie, E. Q. Constructed Uninterrupted Charge-Transfer Pathways in Three-Dimensional Micro/Nanointerconnected Carbon-Based Electrodes for High Energy-Density Ultralight Flexible Supercapacitors. *ACS. Appl. Mater. Interfaces* **2014**, *6*, 210−218.
(45) Michael, R. H.; Scot, T. M.; Wonyong, C.; Detlef, W. B. Environmental Applications of Semiconductor Photocatalysis. *Chem. Rev.* **1995**, *95*, 69−96.
(46) Tian, G. H.; Chen, Y. J.; Ren, Z. Y.; Tian, G. H.; Pan, K.; Zhou, W.; Wang, J. Q.; Fu, H. G. Enhanced Photocatalytic Hydrogen Evolution over Hierarchical Composites of $ZnIn_2S_4$ Nanosheets Grown on MoS_2 Slices. *Chem.—Asian J.* **2014**, *9*, 1291−1297.
(47) Ji, L. W.; Toprakci, O.; Alcoutlabi, M.; Yao, Y. F.; Li, Y.; Zhang, S.; Guo, B. K.; Lin, Z.; Zhang, X. W. α-Fe_2O_3 Nanoparticle-Loaded Carbon Nanofibers as Stable and High-Capacity Anodes for Rechargeable Lithium-Ion Batteries. *ACS. Appl. Mater. Interfaces* **2012**, *4*, 2672−2679.
(48) Toprakci, O.; Ji, L.; Lin, Z.; Toprakci, H. A. K.; Zhang, X. Fabrication and Electrochemical Characteristics of Electrospun $LiFePO_4$/Carbon Composite Fibers for Lithium-Ion Batteries. *J. Power Sources* **2011**, *196*, 7692−7699.
(49) Chen, Y. J.; Huang, R. K.; Chen, D. Q.; Wang, Y. S.; Liu, W. J.; Li, X. N.; Li, Z. H. Exploring the Different Photocatalytic Performance for Dye Degradations over Hexagonal $ZnIn_2S_4$ Microspheres and Cubic $ZnIn_2S_4$ Nanoparticles. *ACS Appl. Mater. Interfaces* **2012**, *4*, 2273−2279.
(50) Chen, Y. M.; Li, X. Y.; Park, K.; Song, J.; Hong, J. H.; Zhou, L. M.; Mai, Y. W.; Huang, H. T.; John, B. G. Hollow Carbon-Nanotube/Carbon-Nanofiber Hybrid Anodes for Li-Ion Batteries. *J. Am. Chem. Soc.* **2013**, *135*, 16280−16283.
(51) Peng, S. J.; Li, L. L.; Wu, Y. Z.; Jia, L.; Tian, L. L.; Srinivasan, M.; Ramakrishna, S.; Yan, Q. Y.; Mhaisalkar, S. G. Size- and Shape-Controlled Synthesis of $ZnIn_2S_4$ Nanocrystals with High Photocatalytic Performance. *CrystEngComm* **2013**, *15*, 1922−1930.
(52) Zhang, M. Y.; Shao, C. L.; Mu, J. B.; Huang, X. M.; Zhang, Z. Y.; Guo, Z. C.; Zhang, P.; Liu, Y. C. Hierarchical Heterostructures of Bi_2MoO_6 on Carbon Nanofibers: Controllable Solvothermal Fabrication and Enhanced Visible Photocatalytic Properties. *J. Mater. Chem.* **2012**, *22*, 577−584.
(53) Yu, J. G.; Ma, T. T.; Liu, G.; Cheng, B. Enhanced Photocatalytic Activity of Bimodal Mesoporous Titania Powders by C_{60} Modification. *Dalton Trans.* **2011**, *40*, 6635−6644.
(54) Yu, J. G.; Fan, J. J.; Cheng, B. Dye-Sensitized Solar Cells Based on Anatase TiO_2 Hollow Spheres/Carbon Nanotube Cmposite Films. *J. Power Sources* **2011**, *196*, 7891−7898.
(55) Zhang, H.; Lv, X. J.; Li, Y. M.; Wang, Y.; Li, J. H. P25-Graphene Composite as a High Performance Photocatalyst. *ACS Nano* **2010**, *4*, 380−386.
(56) Jana, A.; Datta, C. Enhanced Photoelectrochemical Activity of Electro-Synthesized CdS−Bi_2S_3 Composite Films Grown with Self-Designed Cross-Linked Structure. *Electrochim. Acta* **2010**, *55*, 6553−6562.
(57) Li, Q.; Guo, B. D.; Yu, J. G.; Ran, J. R.; Zhang, B. H.; Yan, H. J.; Gong, J. R. Highly Efficient Visible-Light-Driven Photocatalytic Hydrogen Production of CdS-Cluster-Decorated Graphene Nanosheets. *J. Am. Chem. Soc.* **2011**, *133*, 10878−10884.
(58) Zhang, J.; Yu, J. G.; Jaroniec, M.; Gong, J. R. Noble Metal-Free Reduced Graphene Oxide-$Zn_xCd_{1-x}S$ Nanocomposite with Enhanced Solar Photocatalytic H_2-Production Performance. *Nano Lett.* **2012**, *12*, 4584−4589.
(59) Hou, Y. D.; Laursen, A. B.; Zhang, J. S.; Zhang, G. G.; Zhu, Y. S.; Wang, X. C.; Dahl, S.; Chorkendorff, I. Layered Nanojunctions for Hydrogen-Evolution Catalysis. *Angew. Chem., Int. Ed.* **2013**, *52*, 3621−3625.